RSC Advances

PAPER

Cite this: *RSC Adv.*, 2016, **6**, 96538

# Simultaneous topographic and chemical patterning *via* imprinting defined nano-reactors†

Z. Zhao,[a] H. Nan,[a] M. Sun[a] and X. He*[ab]

Simultaneous topographic and chemical patterning has attracted extensive attention in energy harvesting, sensing, and tissue engineering applications. However, it is still challenging to find a universal topographic-chemical patterning method that applies to arbitrary reactions, and offers tunability on the scale of chemical reactions. Herein, we develop a novel strategy to introduce spatially defined ultra-small reactors based on polymer carriers and imprinting lithography to realize simultaneous topographic and chemical patterning. We present two applications to demonstrate the patterning ability of our method, including synthesizing an ultrafine structured layer of photoluminescent Eu(III) complex on polymer substrate, as well as creating a freestanding poly(maleic anyhydride-*alt*-1-octadecene)-polyvinyl alcohol copolymer nanostructure. Further studies show that chemical reactions at polymer interfaces were confined within zepto-liter to atto-liter spaces, which corresponded to $10^3$ to $10^6$ molecules. The scale of chemical reactions can be readily tuned through varying imprinting conditions such as pattern geometry, imprinting time, *etc.* Compared to current patterning techniques, our strategy possesses higher chemical flexibility and compatibility, and allows for better control over the chemical reaction. Not only will this method facilitate fundamental studies of diffusion, reaction dynamics and interfacial chemistry, but it is also highly desired for engineering applications including surface modification, conformal coating and nanofabrication.

Received 4th September 2016
Accepted 4th October 2016

DOI: 10.1039/c6ra22169f

www.rsc.org/advances

## 1. Introduction

The need for simultaneous topographic and chemical patterns has tremendously increased during the past decades. Broad fields such as energy generation,[1–3] chemical/biochemical sensing[4,5] and tissue engineering require highly controlled nanostructures or topography spatially well aligned with specific chemical properties.[6,7] Traditionally, topographic and chemical patterns are generated in a stepwise manner by firstly fabricating a patterned mask or template, followed by surface modifications through physical or chemical deposition,[8,9] imprinting,[10,11] contact printing[12,13] or etching steps.[14] Limitations of these tradition methods, nevertheless, have been widely recognized. Many post-patterning modification approaches possess anisotropic reaction speed and are not able to uniformly modify desired regions.[15,16] In addition, it is usually difficult to handle polymers and biomolecules in the surface modification step as these molecular species may either be incompatible with some reactions conditions, or get geometrically deformed under heat, pressure or electric field.[11,17–20]

Recent development in reactive imprinting lithography (RIL)[21] and reactive contact printing (RCP)[22,23] provides a more efficient, single-step solution to reach simultaneous topographic and chemical patterning for polymer and bio-materials. Both RIL and RCP involve the pre-deposition of a reactive layer that contains all the reactants on the substrate and the trigger of reactions within a stamp process. In one example, furan-masked maleimide polymer films were turned into highly reactive, nanopatterned maleimide-functionalized surfaces *via* retro Diels–Alder reaction in a thermo-imprinting step.[24] In another example, various ligands were immobilized onto a poly(*N*-succinimidyl methacrylate) film in an area selective manner through RCP and used to capture target biomolecules.[23] While considerable success has been achieved by using RIL and RCP, some challenges still exist in those systems, among which the most prominent one is the limitation on the repertoire of reactions. Current functional groups applied in RIL and RCP only support a small selection of reactions, such as click reaction or esterification,[21,24–26] which may not be applicable to desired surface modifications. Meanwhile, multivalent binding process usually experiences incompleteness and high by-product ratios due to limited density and steric effect of the surficial functional groups.[27,28] Moreover, it is almost impossible to control the thickness of chemical patterns, as RIL and RCP technically only apply to the very top molecular layers. As a result, it is highly desirable to develop a universal

[a]*School for Engineering of Matter, Transport and Energy, Arizona State University, Tempe, AZ 85281, USA. E-mail: ximin.he@asu.edu*

[b]*The Biodesign Institute, Molecular Design and Biomimetics Center, Arizona State University, Tempe, AZ 85281, USA*

† Electronic supplementary information (ESI) available. See DOI: 10.1039/c6ra22169f

topographic-chemical patterning method that applies to arbitrary compounds and reactions, and offers tunability on the scale of reactions.

Introducing spatially defined, ultra-small reactors will essentially allow for applying arbitrary reactions at desired locations. However, the fabrication of such reactors usually requires complicate or expensive procedures. Bottom up approaches, for example, employ molecular-scale reactors prepared from the self-assembly of inorganic materials, which is far from easy to implement.[29,30] Top-down methods using microfluidics[31] and "lab-on-a-chip" technology[32] have also been applied in preparing sub-nanoliter reactors. Nevertheless, building up these systems requires complicate steps and costly instrument. Recently, a method of fabricating zeptomole-scale reactors using electrospinned polymer nanofibers was reported.[33] In this work, chemical reagents were loaded inside nanofibers and the reaction was confined in a localized space (ultra-small reactor) by the nanofiber junctions. Alternatively, polymer nano-reactors may also be prepared *via* the dewetting of polymer bilayers.[34,35] Despite their great promise, the spatial accuracy that can be achieved by these electrospinning and dewetting processes is still limited to meet the demands of the ever smaller sub-nanoscale systems nowadays. Hence, new methods with precise control over the product morphology are highly desired.

Herein, we have developed a method that can be exploited to overcome the challenges in current topographic and chemical patterning. This method takes advantage of the precise patterning ability of nanoimprinting[36,37] and the reagent storage/release ability of synthetic polymers. Two polymeric materials are used as chemical carriers in which the reagents are loaded. A double imprinting process has been employed to create desired nanostructures, as well as to spatially control reactions for chemical patterning. During the second imprinting process, chemicals loaded in polymers are able to react at interfaces created by nanoimprinting due to interfacial mixing and molecular diffusion, leading to ultra-small reactors that are of $nm^3$ in size. Two exemplary reactions, namely the synthesis of a multivalent photoluminescent (PL) complex and a crosslinked copolymer, are studied in this work and the structural and chemical information of the products is investigated. The results show that well controlled chemical and topological patterns are able to form *via* this approach. Furthermore, the geometry and thickness of the product layer are also shown to be tunable.

## 2. Experimental

The general schematic of the proposed simultaneous topographic and chemical patterning method is shown in Fig. 1, which is based on imprinting defined nano-reactors. A silicon or perfluopolymer mold was first used to imprint polymer film A, rendering a negative replica of the initial patterns. In the next step, the patterned polymer film A was used to imprint a second polymer film B, which had a slightly lower glass transition temperature ($T_g$). This process yielded nano-structures on

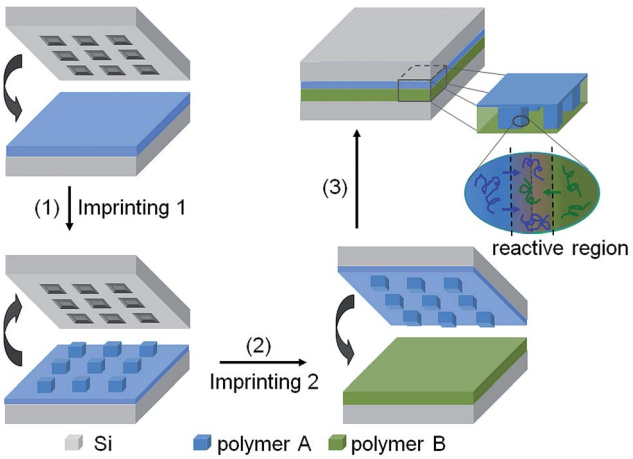


Fig. 1 Scheme of the simultaneous topographic and chemical patterning method. (1) Using Si or ethylene tetrafluoroethylene (ETFE) mold to imprint polymer film A spin cast on a substrate, (2) using the patterned polymer film A as mold to imprint polymer B film, (3) the formation of nano-structured polymer junctions and the chemical patterning generated by localized reactions at interfaces.

polymer B, whose morphology could be tuned through the predesigned pattern in the mother mold and the imprinting conditions. Previous research showed that when nano-sized junction formed between polymeric materials, localized reactions could happen at the polymer interface and yielded ultra-small reactors.[33] Inspired by this, we incorporated reactive species into polymer A and B to complete topographic-chemical patterning in a single step. The nanostructured polymer junction formed in the second imprinting step provided rich nano-reactors where chemical reactions could take place in a geometrically controllable manner.

### 2.1 Mold

Si molds containing line or square hole arrays (patterned area of $2 \times 4$ mm) with each individual feature ranging from 20 nm to 1 μm in width were made by electron-beam lithography and reactive ion etching (RIE), and coated with a self-assembled monolayer of 1*H*,1*H*,2*H*,2*H*-perflurodecyltrichlorosilane by chemical vapor deposition (CVD) as a non-adhesive layer. The groove width in all molds was identical to the width of individual lines/squares while the height of the features was 1 μm for 1 μm wide squares and 80 nm for all the other molds. Ethylene tetrafluoroethylene (ETFE) molds were made by nanoimprinting lithography (Obducat nanoimprinter) from the Si molds and were negative replica of the corresponding Si molds. They were imprinted at 270 °C with 20 bar pressure for 60 min.

### 2.2 Polymer film preparation

Silicon wafers (001) were cleaned by a stepwise ultrasonication in Mili-Q water, acetone, and iso-propanol (15 min for each step), then dried by $N_2$ blow. A treatment in $O_2$ plasma or UV ozone light for 10 minutes was applied to oxidize the surface of Si wafer

before the reagent containing polymeric materials were spin coated. The operation conditions were carefully controlled in the spin coating step as the polymer surface needed to be very smooth and flat to guarantee the conformal contact in the following imprinting steps. Briefly, 1,10-phenanthroline (Phen) and europium(III)thenoyltrifluoroacetonate, trihydrate ($Eu(TTA)_3(H_2O)_3$) purchased from Acros were mixed with poly(vinylpyrrolidinone) (PVP, Aldrich, $M_w = 120$ kg mol$^{-1}$, glass transition temperature $T_g = 127$ °C) in ethanol and polystyrene (PS, Aldrich, $M_w = 125$–$250$ kg mol$^{-1}$, $T_g = 105$ °C) in toluene, respectively. The final concentration was 100 mg L$^{-1}$ : 40 mg L$^{-1}$ for the Phen : PVP mixture and 1 g L$^{-1}$ : 150 mg L$^{-1}$ for the $Eu(TTA)_3$ : PS mixture. The above solutions were spin coated onto Si substrates to render a 110 nm thick **2**:PVP film and a 100 nm thick **1**:PS film for the 25 and 100 nm features, and 1.5 μm thick films for the 1 μm feature. The thicknesses of all polymer films were measured with Dektak profilometer.

### 2.3 Small molecules reaction in polymer matrix

**2**:PVP film was patterned by Si molds at 170 °C and 20 bar pressure for 300 seconds. Subsequently, **1**:PS was imprinted by the pre-patterned **2**:PVP film at 130 °C with 20 bar pressure for 600 seconds. In order to characterize the reaction product at the PS:$Eu(TTA)_3$/PVP:Phen interface, the PVP:Phen layer was removed with ethanol. PL measurement was conducted with pure PVP and PS films, as-cast **1**:PS blend and **2**:PVP blend films, imprinted (**1**:PS)/(**2**:PVP) bilayer films, and also the (**1**:PS)/PVP film for comparison. The PL intensity of the polymer films before and after imprinting was measured by a Varian Cary Eclipse integrated fluorescence spectrophotometer under 347 nm excitation. The surface morphology of Si molds and the imprinted samples were examined with tapping mode AFM (Digital Instruments Nanoscope III). The PS layer was removed by cyclohexane prior to AFM measurements to reveal the underneath PVP structure.

### 2.4 Polymer reaction

100 nm thick poly(maleic anyhydride-*alt*-1-octadecene) (PMAO, Aldrich) and 95 nm thick polyvinyl alcohol (PVA, Aldrich) films were spin coated on Si substrates. First, PMAO film was imprinted by 2-D Si mold containing 100 nm wide, 80 nm deep holes at 170 °C with 20 bar pressure for 300 s. Subsequently, PVA film was imprinted by the patterned PMAO film at 100 °C with 20 bar pressure applied for 5 min or 40 min, followed by an additional 25 minute cooling before removing the mold. In order to check the interface of the imprinted PMAO/PVA blend film, the bilayer sample was first soaked in 90 °C water bath for 30 min, and then immersed in 60 °C toluene for 30 min to remove PVA and PMAO, respectively. The surface morphology of Si molds and the imprinted samples were examined with tapping mode AFM. The chemical composition of the reaction products was examined by Fourier transform infrared spectroscopy (FT-IR, Bruker IFS66V/S) in transmission mode.

## 3. Results and discussion

### 3.1 Double-imprinting defined nano-reactors

The feasibility and replication fidelity along with the patterning quality of the double imprinting method mentioned in Fig. 1 were tested by a series of experiments. Patterned PVP films were used as molds to imprint PS films. Uniform ultra-small features down to 20 nm were successfully obtained in polymeric materials after the double-imprinting steps, confirming the decent topological patterning ability of our technique (Fig. 2). Note the bending and distortion of PVP pillars in Fig. 2c were due to the mechanical instability during the wash steps before imaging. More experimental results, as well as detailed experimental conditions could be found in the ESI (Fig. S1 & S2†). Notably, this double imprinting procedure should be valid for any polymer combinations regardless of their chemical properties, mutual interactions and molecular weights provided there existed a difference in $T_g$ between the two materials. To prove this, we tested immiscible polymer pair polystyrene (PS)/polyethylene oxide (PEO) and miscible polymer pair polymethyl methacrylate (PMMA)/PEO. Both systems successfully yielded regular nanostructures after the double imprinting (Fig. S3†), indicating the excellent material compatibility of the topological patterning.

### 3.2 Formation of nano-structured $Eu(Phen)(TTA)_3$ layer

To demonstrate the chemical patterning capability, we studied a couple of proof of principle reactions. A photoluminescent (PL) Eu complex, $Eu(Phen)(TTA)_3$, was first synthesized (Phen = 1,10-phenanthroline, TTA = thenoyltrifluoroacetonate), which has been widely used in organic light emitting devices as a dopant light emitter.[38,39] To complete the synthetic reaction, we spin coated phenanthroline-doped polyvinylpyridine (**2**:PVP) film and $Eu(TTA)_3$ doped PS (**1**:PS) film onto separate substrates and imprinted them to create a nanostructured polymer interface, at which the complexation reaction could occur (Fig. 3a). Significant increase in the fluorescent signal was observed when a flat **1**:PS was imprinted by the pre-nanostructured **2**:PVP film containing europium reagent for all the pattern geometry we tested (Fig. 3b). In contrast to the initial weak emission of **1**:PS film, a stronger peak was seen at ~615 nm after the imprinting, which was due to the higher quantum yield of the $Eu(Phen)(TTA)_3$ compound.[40] This confirmed that the two reactants (**1** and **2**) physically-mixed with polymer carriers were able to diffuse across the interface and undergo chemical reactions, resulting in the generation of **3**, a strongly PL compound.

We observed that when the feature size decreased from 1 μm to 100 nm and 25 nm, the overall PL intensity increased from 2 fold to 3.3 and 7.1 fold of the initial **1**:PS PL intensity, respectively. This geometry-dependent photoluminescence was believed to be determined by the total area of interfaces, as well as the size of each individual nano-features. A geometrical calculation was conducted by assuming that the complexation reaction happened at the same rate across the whole interface (Fig. S4†). The result showed that the quantity of the final product was proportional to

 

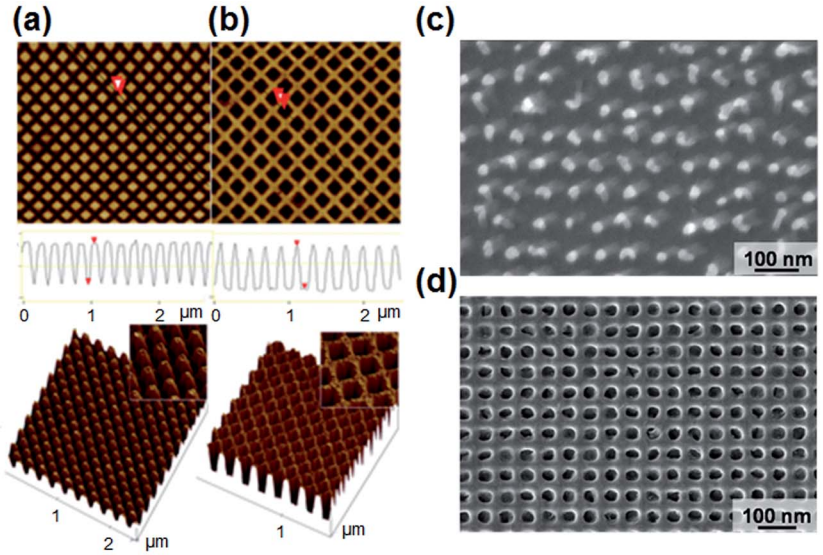


Fig. 2 (a) AFM images of a patterned PVP film after imprinting PS films. (b) AFM image of a PS film imprinted by the PVP mold in (a). (c) SEM image of a PVP pillar array after imprinting PS films. (d) SEM image of a hole array in PS film created by the PVP mold in (c).

the aspect ratio (AR) of the nano-feature, which was defined as the feature height over the feature width. This explained why the 25 nm feature possessed the highest PL intensity (AR = 5). On the other hand, we found that the measured PL intensity was also affected by the imprinting process. A slight reduction in the PL intensity was observed when the **1**:PS film was imprinted by pure PVP with 1 μm squares (Fig. 3b). This phenomenon was attributed to the loss of PL emission during transmission in the nano-structured polymer (*e.g.* diffusive reflection, scattering, *etc.*). In this case, the total signal loss due to imprinting should be proportional to the thickness of the material. Consequently, we observe a higher PL intensity in 100 nm features (80 nm thick) although the 1 μm feature possessed slightly higher aspect ratio (1 μm thick).

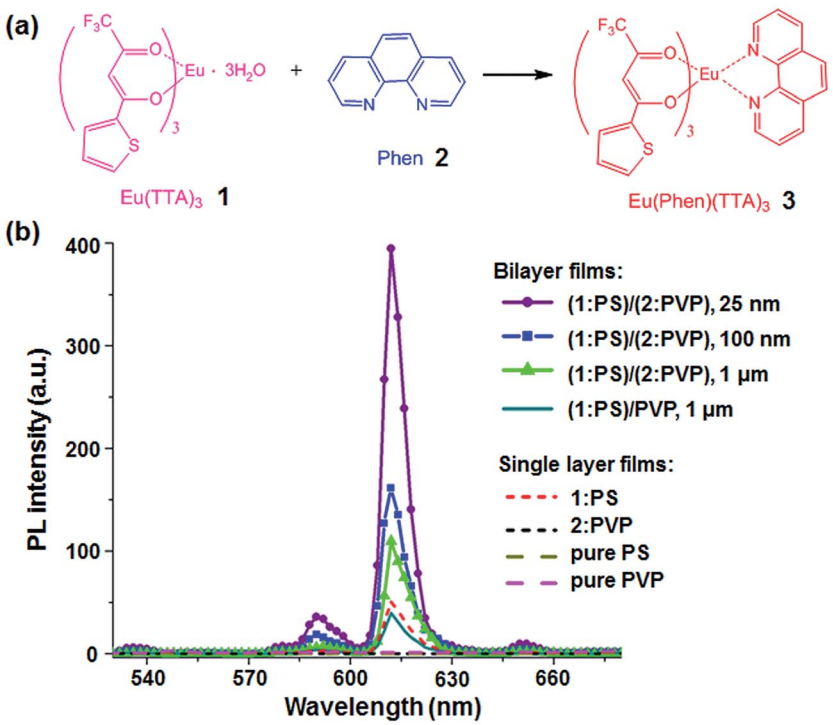


Fig. 3 (a) The reaction equation of synthesizing Eu(Phen)$(TTA)_3$ (**3**) from Eu$(TTA)_3$ (**1**) and Phen (**2**). (b) Photoluminescence of single layer polymer films and imprinted bilayer polymers films. Single layer films: pristine PVP, pristine PS, **2**:PVP film and **1**:PS film. Bilayer films: **1**:PS film imprinted by **2**:PVP with 25 nm, 100 nm and 1 μm square patterns, and **1**:PS film imprinted by prepatterned pure PVP film.

To further investigate the chemical patterning process, we collected AFM profiles of the nanostructured **2**:PVP surface before and after imprinting **1**:PS (Fig. 4a–i). It was found that the average height of square features was increased by ~5 nm in all cases. The increased thickness indicated that the deposition of $Eu(Phen)(TTA)_3$ happened during the imprinting process and the product was stable enough to withstand solvent wash for PS removal. Based on the size of each nano-square and the thickness of the deposition layer, we calculated the apparent volume of each reactor. Reactors of $5.41 \times 10^4$ nm$^3$, $2.29 \times 10^5$ nm$^3$, and $2.52 \times 10^7$ nm$^3$ were formed for 25 nm, 100 nm, and 1 μm squares, respectively, which corresponded to 54.1 zL, 229 zL and 25.2 aL reactors. With the concentration of **1** and **2** of about 0.17 mmol mL$^{-1}$ in the film, we knew that approximately 9.3 zeptomole-4.6 attomole, or $5.6 \times 10^3$ to $2.8 \times 10^6$ molecules were involved in the reactions. The result demonstrated that it was possible to create ultra-small reactors of desired shape through imprinting and the size of reactors was able to be tuned by up to $10^4$ fold by changing the feature size. Further tuning of the number of reagent molecules in each reactor might be achieved by adjusting the reactant concentration in the polymer carrier.

### 3.3 Synthesis of polymer nanostructures with the nanoreactors

The above example illustrated the capability of conducting small molecule reactions involving multivalent complexation, which was difficult to achieve with conventional contact printing or imprinting methods. To further demonstrate the advantages of our technique, we conducted macromolecule reactions between polymers. It has been known that larger molecules typically have greater difficulty diffusing through matrices. However, the diffusion process can be significantly enhanced with the assistance of heat or solvent,[41,42] which makes it possible to directly conduct polymeric reactions in the double imprinting steps. Herein, we explored the feasibility and dynamics of the crosslinking reaction between two polymers that carried complementary reactive groups. By doing nanoimprinting, a nanostructured copolymer was expected to form and covalently bound to the base material. To do this, we first spin coated poly(maleic anyhydride-*alt*-1-octadecene) (PMAO, $M_n$ 30–50 kg mol$^{-1}$, $T_g$ 120–130 °C) and polyvinyl alcohol (PVA, $M_n$ 31–50 kg mol$^{-1}$, $T_g$ 70–80 °C) onto separate substrates. The initial Si mold contained 100 nm square hole array and was used to imprint PMAO. Next, the PVA film was imprinted by PMAO to trigger the crosslinking reaction (Fig. 5a).

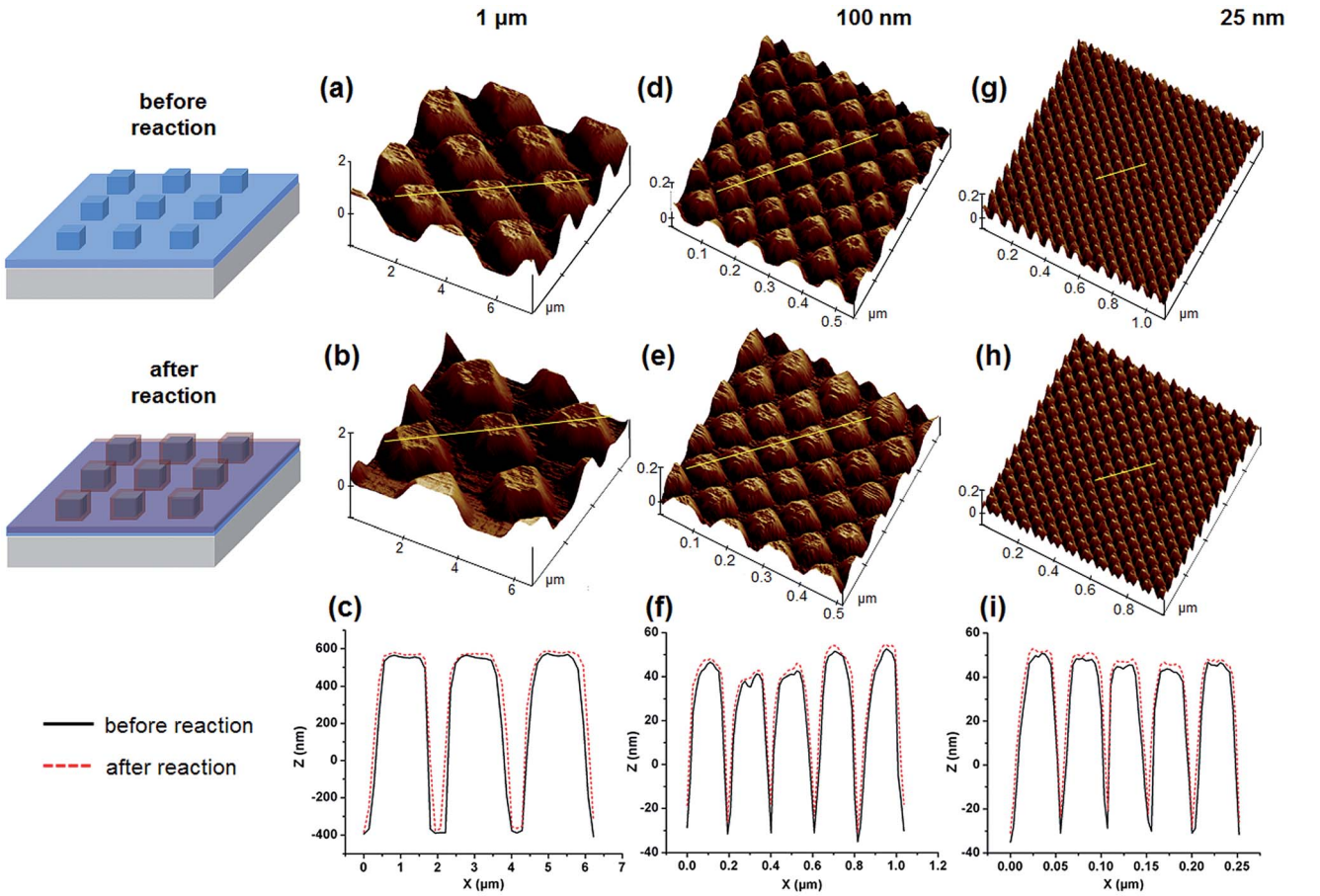


Fig. 4 AFM images and cross-sectional profiles of (a)–(c) 1 μm, (d)–(f) 100 nm and (g)–(i) 25 nm wide **2**:PVP square arrays before and after imprinting, with **1**:PS layer removed in (b), (c), (e), (f), (h) and (i) to reveal the surface of **2**:PVP. The black solid curves and red dashed curves in the cross-sectional images represent AFM profiles of the corresponding yellow lines indicated in the AFM topographies before and after reactions.

In order to quantify the crosslinking at the interface, the as-produced bilayer polymer was soaked in water and toluene to remove PVA and PMAO. The remaining material was subsequently examined by SEM and FT-IR for morphology and composition studies, respectively. It was found that the remaining nanostructures left on the substrate were insoluble in either water or toluene, indicating that cross-linking between PVA and PMAO did occur during imprinting. The FT-IR spectra were used to confirm the composition of the newly formed nanostructures. As shown in Fig. 5b, the anhydride peak at 1778 $cm^{-1}$ and 1709 $cm^{-1}$ almost disappeared after the imprinting and the 1707 $cm^{-1}$ peak was enhanced, which was attributed to the carboxyl and ester groups in **6**.[43] Meanwhile, the OH stretching at ~3200 $cm^{-1}$ became more intense, further confirming the generation of carboxyl groups.

We observed that imprinting time played a key role in determining the thickness of product. PMAO-PVA structure formed after 40 minute imprinting appeared to be thicker and broader compared with that obtained by 5 minutes, indicating more products were yielded (Fig. 5c *vs.* d). The AFM cross section profiles (Fig. 5e–g) further confirmed the influence of imprinting time on the thickness of reaction zones. We found the measured average width of the square post changed to 106 nm and 115 nm for 5 min and 40 minute imprinting, which corresponded to 40 zL and 100 zL reaction volumes, respectively. This change was mainly due to the longer diffusion length of polymers under extended heating time. In this way, zepto- to nano-scaled reactors can be readily generated by simply controlling the imprinting time, and the thickness of the chemical patterning can be adjusted.

# 4. Conclusions

We have demonstrated a universal and high-throughput strategy to simultaneously create topographic and chemical patterns. This method employed polymeric materials as carriers of reactive species, which were turned into ultra-small reactors in the nanoimprinting step. The topological structures generated by imprinting provided a nanoscale reservoir from which reagents in one carrier could diffuse and react with molecules loaded in the opposite side. We presented two applications to demonstrated the chemical patterning ability of our method, including synthesizing a PL Eu(III) complex layer on polymer substrate, as well as creating a crosslinked, freestanding copolymer nanostructure. Further studies showed that chemical reactions were confined in zepto-liter to atto-liter spaces, which corresponded to $10^3$ to $10^6$ molecules. The reactive molecules in each reactor were determined by the original size of the surface structure, but also influenced by reaction conditions such as imprinting time and reactant concentrations. Therefore, it was possible to finely tune the thickness of the product while maintain a consistent topological structure.

Compared to previously developed patterning techniques, our method possesses several advantages. First, the abundance of polymer carriers make it possible to conduct almost any types of reactions for chemical patterning, rendering excellent flexibility and compatibility that are impossible to realize in current patterning techniques. The use of nanoimprinting allowes the reagents to react in a synchronized fashion so as to achieve eliminated dispersion and better control over the chemistry. Importantly, the facile molding process also readily allowes for

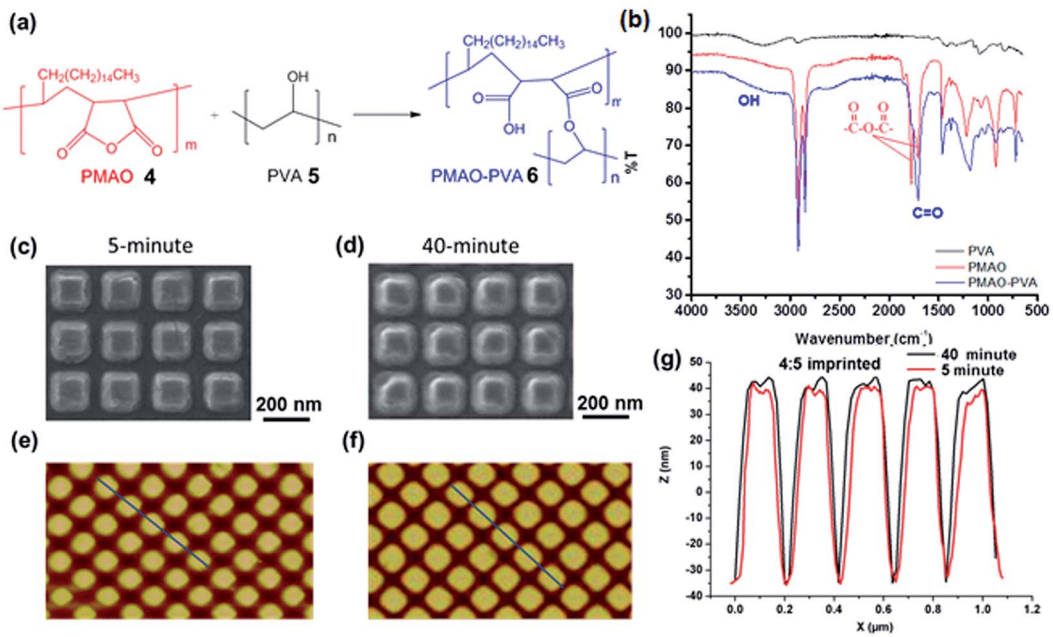


Fig. 5 (a) Reaction between PMAO and PVA taking place at the nanostructured interface of these two polymers. (b) FT-IR spectra of pristine PMAO, pristine PVA and the PMAO/PVA interface after nanoimprinting. SEM images of the interfaces of nanoimprinted polymer blend of PMAO:PVA containing 100 nm wide square dots for (c) 5- and (d) 40 minute imprinting. (e) and (f) are AFM topological images corresponding to (c) and (d). Figure (g) is the cross-sectional profile of (e) and (f).

precise control of the reaction scale at nanometer resolution, which was hard to achieve in other surface modification techniques. With future design of surface patterns, this platform may be use to complete multiple reactions in parallel by depositing various reagents at different regions.[44,45] Many applications can be derived from the presented work. Not only will it facilitate fundamental studies of diffusion, reaction dynamics and interfacial chemistry, but it is also highly desired for engineering applications including surface modification, conformal coating and nanofabrication.

## Acknowledgements

We thank the Nanoscience Center of University of Cambridge for the nanofabrication facilities. We are grateful of the valuable discussions with Dr Wilhelm Huck on this work.

## References

1 X. He, F. Gao, G. Tu, D. G. Hasko, S. Hüttner, N. C. Greenham, U. Steiner, R. H. Friend and W. T. S. Huck, *Adv. Funct. Mater.*, 2011, **21**, 139–146.
2 J. E. Slota, X. He and W. T. S. Huck, *Nano Today*, 2010, **5**, 231–242.
3 X. He, F. Gao, G. Tu, D. Hasko, S. Hüttner, U. Steiner, N. C. Greenham, R. Friend and W. Huck, *Nano Lett.*, 2010, **10**, 1302–1307.
4 E. Phizicky, P. I. Bastiaens, H. Zhu, M. Snyder and S. Fields, *Nature*, 2003, **422**, 208–215.
5 C. N. LaFratta and D. R. Walt, *Chem. Rev.*, 2008, **108**, 614–637.
6 H. Hatakeyama, A. Kikuchi, M. Yamato and T. Okano, *Biomaterials*, 2007, **28**, 3632–3643.
7 A. Khademhosseini and R. Langer, *Biomaterials*, 2007, **28**, 5087–5092.
8 W. S. Liao, H. H. Cao, S. Cheunkar, M. J. Shuster, S. C. Altieri, P. S. Weiss and A. M. Andrews, *J. Phys. Chem. C*, 2013, **117**, 22362–22368.
9 T. R. Jensen, M. D. Malinsky, C. L. Haynes and R. P. Van Duyne, *J. Phys. Chem. B*, 2000, **104**, 10549–10556.
10 Y. Cai, Z. Zhao, J. Chen, T. Yang and P. S. Cremer, *ACS Nano*, 2012, **6**, 1548–1556.
11 X. He, J. Winkel and W. T. S. Huck, *Adv. Mater.*, 2009, **21**, 2083–2087.
12 J. P. Renault, A. Bernard, D. Juncker, B. Michel, H. R. Bosshard and E. Delamarche, *Angew. Chem.*, 2002, **114**, 2426–2429.
13 W. S. Liao, S. Cheunkar, H. H. Cao, H. R. Bednar and P. S. Weiss, *Science*, 2012, **337**, 1517–1521.
14 Z. Zhao, Y. Cai, W. S. Liao and P. S. Cremer, *Langmuir*, 2013, **29**, 6737–6745.
15 Y. H. Lee and M. M. Chen, *J. Appl. Phys.*, 1983, **54**, 5966–5973.
16 S. Franssila, *Introduction to microfabrication*, John Wiley & Sons, Hoboken, 2010.
17 K. M. Midthun, P. G. Taylor, C. Newby, M. Chatzichristidi, P. S. Petrou, J. K. Lee, S. E. Kakabakos, B. A. Baird and C. K. Ober, *Biomacromolecules*, 2013, **14**, 993–1002.
18 B. D. Ratner, A. S. Hoffman, F. J. Schoen and J. E. Lemons, *Biomaterials science: an introduction to materials in medicine*, Academic press, Cambridge, 2004.
19 M. Park, C. K. Harrison, P. M. Chaikin, R. A. Register and D. H. Adamson, *Science*, 1997, **276**, 1401–1404.
20 Z. Lin, T. Kerle, T. P. Russell, E. Schaeffer and U. Steiner, *Macromolecules*, 2002, **35**, 6255–6262.
21 J. Duvigneau, S. Cornelissen, N. Bardají Valls, H. Schönherr and G. J. Vancso, *Adv. Funct. Mater.*, 2010, **20**, 460–468.
22 H. Schönherr, C. Feng and A. Shovsky, *Langmuir*, 2003, **19**, 10843–10851.
23 C. L. Feng, G. J. Vancso and H. Schönherr, *Adv. Funct. Mater.*, 2006, **16**, 1306–1312.
24 C. Subramani, N. Cengiz, K. Saha, T. N. Gevrek, X. Yu, Y. Jeong, A. Bajaj, A. Sanyal and V. M. Rotello, *Adv. Mater.*, 2011, **23**, 3165–3169.
25 B. Dordi, H. Schönherr and G. J. Vancso, *Langmuir*, 2003, **19**, 5780–5786.
26 N. Gupta, B. F. Lin, L. M. Campos, M. D. Dimitriou, S. T. Hikita, N. D. Treat, M. V. Tirrell, D. O. Clegg, E. J. Kramer and C. J. Hawker, *Nat. Chem.*, 2010, **2**, 138–145.
27 V. M. Krishnamurthy, L. A. Estroff and G. M. Whitesides, *Fragment-based approaches in drug discovery*, Wiley & Sons, Hoboken, 2006.
28 W. S. Hlavacek, R. G. Posner and A. S. Perelson, *Biophys. J.*, 1999, **76**, 3031–3043.
29 J. Fan, W. Shui, P. Yang, X. Wang, Y. Xu, H. Wang, X. Chen and D. Zhao, *Chem.–Eur. J.*, 2005, **11**, 5391–5396.
30 Y. D. Tretyakov, A. V. Lukashin and A. A. Eliseev, *Russ. Chem. Rev.*, 2004, **73**, 899–921.
31 G. M. Whitesides, *Nature*, 2006, **442**, 368–373.
32 N. T. Nguyen and S. T. Wereley, *Fundamentals and applications of microfluidics*, Artech House, Norwood, 2002.
33 P. Anzenbacher and M. A. Palacios Jr, *Nat. Chem.*, 2009, **1**, 80–86.
34 S. C. Thickett, C. Neto and A. T. Harris, *Adv. Mater.*, 2011, **23**, 3718–3722.
35 A. M. Telford, S. C. Thickett, M. James and C. Neto, *Langmuir*, 2011, **27**, 14207–14217.
36 S. Y. Chou, P. R. Krauss and P. J. Renstrom, *Appl. Phys. Lett.*, 1995, **67**, 3114–3116.
37 S. Y. Chou, P. R. Krauss and P. J. Renstrom, *Science*, 1996, **272**, 85.
38 M. Hu, Z. Huang, Y. Cheng, S. Wang, J. Lin, Y. Hu, D. Xu and Y. Xu, *Chin. J. Chem.*, 1999, **17**, 637–643.
39 J. Kido and Y. Okamoto, *Chem. Rev.*, 2002, **102**, 2357–2368.
40 P. K. Shahi, A. K. Singh, S. K. Singh, S. B. Rai and B. Ullrich, *ACS Appl. Mater. Interfaces*, 2015, **7**, 18231–18239.
41 K. C. Tseng, N. J. Turro and C. J. Durning, *Phys. Rev. E*, 2000, **61**, 1800.
42 G. D. Verros and N. A. Malamataris, *Macromol. Theory Simul.*, 2001, **10**, 737–749.
43 W. W. Yu, E. Chang, J. C. Falkner, J. Zhang, A. M. Al-Somali, C. M. Sayes, J. Johns, R. Drezek and V. L. Colvin, *J. Am. Chem. Soc.*, 2007, **129**, 2871–2879.
44 S. Hong, J. Zhu and C. A. Mirkin, *Science*, 1999, **286**, 523–525.
45 P. Calvert, *Chem. Mater.*, 2001, **13**, 3299–3330.

 